J|A|C|S
ARTICLES
Published on Web 09/25/2004

# Photocatalytic $H_2$ Evolution Reaction from Aqueous Solutions over Band Structure-Controlled $(AgIn)_xZn_{2(1-x)}S_2$ Solid Solution Photocatalysts with Visible-Light Response and Their Surface Nanostructures

Issei Tsuji,[†] Hideki Kato,[†] Hisayoshi Kobayashi,[‡] and Akihiko Kudo*[,†,§]

*Contribution from the Department of Applied Chemistry, Faculty of Science, Science University of Tokyo, 1-3 Kagurazaka, Shinjuku-ku, Tokyo 162-8601, Japan, Department of Chemistry and Bioscience, Faculty of Chemical Technology, Kurashiki University of Science and the Arts, 2640 Nishinoura, Tsurajima, Kurashiki 712-8505, Japan, and Core Research for Evolutional Science and Technology, Japan Science and Technology Agency (CREST, JST), 4-1-8 Honcho, Kawaguchi-shi, Saitama 332-0012*

Received March 24, 2004; E-mail: a-kudo@rs.kagu.tus.ac.jp

***Abstract:*** $(AgIn)_xZn_{2(1-x)}S_2$ solid solutions between ZnS photocatalyst with a wide band gap and $AgInS_2$ with a narrow band gap showed photocatalytic activities for $H_2$ evolution from aqueous solutions containing sacrificial reagents, $SO_3^{2-}$ and $S^{2-}$, under visible-light irradiation ($\lambda \geq 420$ nm) even without Pt cocatalysts. Loading of the Pt cocatalysts improved the photocatalytic activity. Pt (3 wt %)-loaded $(AgIn)_{0.22}Zn_{1.56}S_2$ with a 2.3 eV band gap showed the highest activity for $H_2$ evolution, and the apparent quantum yield at 420 nm amounted to 20%. $H_2$ gas evolved at a rate of 3.3 L $m^{-2}$•$h^{-1}$ under irradiation using a solar simulator (AM 1.5). The diffuse reflection and the photoluminescence spectra of the solid solutions shifted monotonically to a long wavelength side as the ratio of $AgInS_2$ to ZnS increased in the solid solutions. The photocatalytic $H_2$ evolution depended on the compositions as well as the photophysical properties. The dependence of the photophysical and photocatalytic properties upon the composition was mainly due to the change in the band position caused by the contribution of the Ag 4d and In 5s5p orbitals to the valence and conduction bands, respectively. It was found from SEM and TEM observations that the solid solutions partially had nanostep structures on their surfaces. The Pt cocatalysts were selectively photodeposited on the edge of the surface nanosteps. It was suggested that the specific surface nanostructure was effective for the suppression of recombination between photogenerated electrons and holes and for the separation of $H_2$ evolution sites from oxidation reaction sites.

## Introduction

Development of visible-light-driven photocatalysts that produce hydrogen from water using solar light energy has been urged for shifting to a hydrogen energy system. However, a highly efficient photocatalyst for overall water splitting under visible-light irradiation has never been developed. Pt-loaded CdS (2.4 eV) is a well-known photocatalyst for producing hydrogen from aqueous solutions containing sacrificial reagents.[1,2]

It is indispensable to control the energy structure for the development of visible-light-driven photocatalyst materials. The strategy for the design of photocatalyst materials with visible-light response is classified in three ways, as shown in Figure 1. Strategy (a) is the doping of foreign elements into active photocatalysts with a wide band gap to form donor levels in the forbidden band. $TiO_2$ and $SrTiO_3$ codoped with Sb or Ta and Cr,[3,4] ZnS doped with Cu or Ni,[5,6] and ZnS codoped with Pb and halogens[7] have been reported as active powdered photocatalysts. Especially, the Ni or Cu-doped ZnS photocatalyst

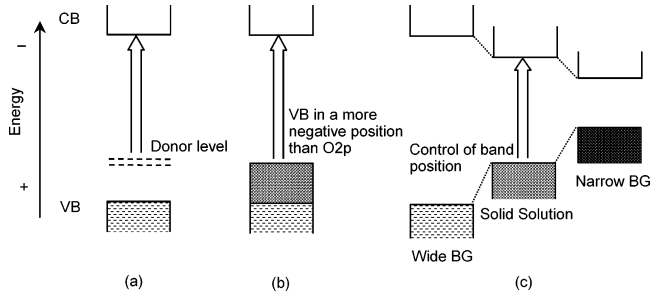


***Figure 1.*** Band engineering for design of photocatalyst materials with visible-light response. (a) Donor level formation by doping of foreign elements, (b) new stable valence band formation in a more negative position, and (c) a controllable band formation by making a solid solution.

[†] Science University of Tokyo.
[‡] Kurashiki University of Science and the Arts.
[§] Japan Science and Technology Agency.

(1) Matsumura, M.; Furukawa, S.; Saho, Y.; Tsubomura, H. *J. Phys. Chem.* **1985**, *89*, 1327−1329.
(2) Reber, J. F.; Meier, K. *J. Phys. Chem.* **1986**, *90*, 824−834.
(3) Kato, H.; Kudo, A. *J. Phys. Chem. B* **2002**, *106*, 5029−5034.
(4) Ishii, T.; Kato, H.; Kudo, A. *J. Photochem. Photobiol., A* **2004**, *163*, 181−186.
(5) Kudo, A.; Sekizawa, M. *Catal. Lett.* **1999**, *58*, 241−243.
(6) Kudo, A.; Sekizawa, M. *Chem. Commun.* **2000**, 1371−1372.
(7) Tsuji, I.; Kudo, A. *J. Photochem. Photobiol., A* **2003**, *156*, 249−252.


**10.1021/ja048296m CCC: $27.50** 

shows a high activity for $H_2$ evolution under visible-light irradiation even without a Pt cocatalyst. Thus, doping of foreign elements is effective for the construction of visible-light-driven photocatalyst materials in some cases. However, it has some problems in that the doping levels formed in a forbidden band are generally discrete and also that the mobility of the electron and hole in the doping levels is low. Moreover, there is difficulty in absorbing a sufficient quantity of visible light by transitions due to the doping levels. Strategy (b) is to find materials that have a stable valence band in a more negative position than the valence band consisting of O 2p orbitals, as seen in many oxide photocatalysts. $BiVO_4$ and $AgNbO_3$ are visible-light-driven photocatalysts for $O_2$ evolution.[8−11] Their valence bands consist of hybrid orbitals of Bi 6s or Ag 4d with O 2p orbitals and possess enough potential to oxidize $H_2O$ to form $O_2$ with four-electron oxidation in an aqueous solution containing $Ag^+$ of an electron scavenger. Nitride and oxynitride compounds such as $Ta_3N_5$,[12] TaON,[13] and $LaTiO_2N$,[14] and an oxysulfide, $Sm_2Ti_2S_2O_5$,[15] have been reported as active photocatalysts that have valence bands consisting of N 2p orbitals and hybrid orbitals of N 2p or S 3p with O 2p orbitals, respectively. Strategy (c) is the control of the energy structure by making solid solutions between semiconductor photocatalysts with wide and narrow band gaps. The photophysical properties and photocatalytic activities of $Nb_2O_5-Bi_2O_3$,[16] $Ga_2O_3-In_2O_3$,[17] $Sr_2Nb_2O_7-Sr_2Ta_2O_7$,[18,19] $SnO_2-TiO_2$,[20] ZnS−CdS,[2,21,22] and CdS−CdSe[23,24] solid solutions are dependent on their compositions.

ZnS is an interesting photocatalyst material from the viewpoint of its preeminent ability to produce $H_2$. ZnS with a wide band gap (3.5 eV) is a highly active photocatalyst for $H_2$ evolution even without Pt cocatalysts under ultraviolet-light irradiation, because the conduction band level is high enough for a reduction potential of $H_2O$ to form $H_2$.[25,26] The ZnS photocatalyst is a good host material for development of a visible-light-driven photocatalyst by the doping of foreign elements, as mentioned above.[5−7] ZnS is also able to form $(AgIn)_xZn_{2(1-x)}S_2$ solid solutions with a narrow band gap semiconductor, $AgInS_2$.[27,28] The solid solutions include Ag that is expected to contribute to valence band formation as observed for an $AgNbO_3$ photocatalyst.[11]

These facts have motivated us to investigate the photophysical and photocatalytic properties of $(AgIn)_xZn_{2(1-x)}S_2$ solid solutions. We preliminarily reported that the $(AgIn)_{0.22}Zn_{1.56}S_2$ (= $AgInZn_7S_9$) solid solution showed high activity for $H_2$ evolution under visible-light irradiation.[29] In the present article, we report the relationships among the systematically studied photophysical properties, photocatalytic activities, and band structure of $(AgIn)_xZn_{2(1-x)}S_2$ solid solutions, and the role of surface morphology is also discussed. $H_2$ production in $(AgIn)_xZn_{2(1-x)}S_2$ solid solutions was demonstrated using a solar simulator (AM 1.5).

## Experimental Section

**Preparation and Characterization of Photocatalysts.** A grayish precipitate of a Ag−In−Zn sulfide precursor was prepared by bubbling a $H_2S$ gas into the mixed aqueous solution of $AgNO_3$ (Tanaka Kikinzoku; 99.8%), $In(NO_3)_3 \cdot 3.9H_2O$ (Kojundo Chemical; 99.99%), and $Zn(NO_3)_2 \cdot 6H_2O$ (Wako Pure Chemicals; 99.0%) in a stoichiometric molar ratio or with excess amounts of several percents of indium. The precipitate was washed with pure water and dried in air. The obtained powder was heat-treated at 1123 K for 5 h in an $N_2$ flow or an evacuated quartz ampule tube. The product phases were confirmed by X-ray diffraction (Rigaku; MiniFlex). Surface areas were determined by the $N_2$ BET method (Coulter; SA3100). Diffuse reflection spectra were obtained using a UV−vis−NIR spectrometer (Jasco; Ubest U-570) and were converted from reflection to absorbance by the Kubelka−Munk method. Photoluminescence spectra were measured in vacuo at 80 K using a spectrofluorometer (Spex; FluoroMax). Photocatalyst powders were observed by scanning (JEOL; JSM-7400F, Hitachi; S-5000) and transmission electron microscopes (JEOL; JEM-2000F).

**Photocatalytic Reactions.** Photocatalytic reactions were conducted in a gas-closed circulation system with a side or top window Pyrex cell. The photocatalyst powder (0.3 g) was dispersed by a magnetic stirrer in an aqueous solution (150−300 mL) containing $K_2SO_3$ and/or $Na_2S$ as electron donors. The photocatalysts were irradiated with visible light ($\lambda \geq 420$ nm) through a cutoff filter (HOYA; L42) from a 300 W Xe lamp (ILC technology; CERMAX LX-300). A solar simulator (YAMASHITA DENSO; YSS-80QA) was also used for the test of the photocatalytic reaction under simulated sunlight irradiation (AM 1.5). Pt cocatalysts were loaded by a photodeposition method in situ. An aqueous solution containing an appropriate amount of $H_2PtCl_6$ (Tanaka Kikinzoku; 37.55% as Pt) was added in the reactant solution. The activity of the CdS (Kojundo-kagaku; 99.99%) photocatalyst was examined as a reference. The amount of an evolved $H_2$ gas was determined using online gas chromatography (Shimadzu; GC-8A, MS-5A column, TCD, Ar carrier). Apparent quantum yields defined by the following equation were measured using filters combined with band-pass (Kenko) and cutoff (HOYA) filters and a photodiode (OPHIRA: PD300-UV of a head and NOVA of a power monitor).

$$\text{A.Q.Y.}(\%) = \frac{\text{The number of reacted electrons}}{\text{The number of incident photons}} \times 100$$

$$= \frac{\text{The number of evolved } H_2 \text{ molecules} \times 2}{\text{The number of incident photons}} \times 100$$

**Band Structure Calculation.** The plane-wave-based density functional theory (DFT) calculation was carried out for ZnS with wurtzite structure and $AgInS_2$ with a wurtzite-like structure by employing the


(8) Kudo, A.; Ueda, K.; Mikami, I. *Catal. Lett*. **1998**, 391−392.
(9) Kudo, A.; Omori, K.; Kato, H. *J. Am. Chem. Soc*. **1999**, *121*, 11459−11467.
(10) Tokunaga, H.; Kato, H.; Kudo, A. *Chem. Mater*. **2001**, *13*, 4624−4628.
(11) Kato, H.; Kobayashi, H.; Kudo, A. *J. Phys. Chem*. **2002**, *106*, 12441−12447.
(12) Hara, M.; Hitoki, G.; Takata, T.; Kondo, J. N.; Kobayashi, H.; Domen, K. *Stud. Surf. Sci. Catal*. **2003**, *145*, 169−172.
(13) Hara, M.; Hitoki, G.; Takata, T.; Kondo, J. N.; Kobayashi, H.; Domen, K. *Catal. Today*. **2003**, *78*, 555−560.
(14) Kasahara, A.; Nukumizu, N.; Takata, T.; Kondo, J. N.; Hara, M.; Kobayash, H.; Domen, K. *J. Phys. Chem. B* **2003**, *107*, 791−797.
(15) Ishikawa, A.; Takata, T.; Kondo, J. N.; Hara, M.; Kobayashi, K.; Domen, K. *J. Am. Chem. Soc*. **2002**, *124*, 13547−13553.
(16) Harriman, A.; Thomas, J. M.; Zhou, W.; Jefferson, D. A. *J. Solid State Chem*. **1988**, *72*, 126−130.
(17) Kudo, A.; Mikami, I. *J. Chem. Soc., Faraday Trans*. **1998**, *94*, 2929−2932.
(18) Kato, H.; Kudo, A. *J. Photochem. Photobiol., A* **2001**, *145*, 129−133.
(19) Yoshino, M.; Kakihana, M.; Seok, C. W.; Kato, H.; Kudo, A. *Chem. Mater*. **2002**, *14*, 3369−3376.
(20) Lin, J.; Yu, J. C.; Lo, D.; Lam, S. K. *J. Catal*. **1999**, *183*, 368−372.
(21) Youn, H. C.; Baral, S.; Fendler, J. H. *J. Phys. Chem*. **1988**, *92*, 6320−6327.
(22) Inoue, H.; Moriwaki, H.; Maeda, K.; Yoneyama, H. *J. Photochem. Photobiol., A* **1995**, *86*, 191−196.
(23) Kambe, S.; Fujii, M.; Kawai, T.; Kawai, S. *Chem. Phys. Lett*. **1984**, *109*, 105−109.
(24) Uchihara, T.; Abe, H.; Matsumura, M.; Tsubomura, H. *Bull. Chem. Soc. Jpn*. **1989**, *62*, 1042−1046.
(25) Reber, J.; Meier, F. K. *J. Phys. Chem*. **1984**, *88*, 5903−5913.
(26) Zeug, N.; Bücheler, J.; Kisch, H. *J. Am. Chem. Soc*. **1985**, *107*, 1495−1465.
(27) Lambrecht, V. G., Jr. *Mater. Res. Bull*. **1972**, *7*, 1411−1415.
(28) Olekseyuk, I. D.; Halka, V. O.; Parasyuk, O. V.; Voronyuk, S. V. *J. Alloys Compd*. **2001**, *325*, 204−209.
(29) Kudo, A.; Tsuji, I.; Kato, H. *Chem. Commun*. **2002**, 1958−1959.

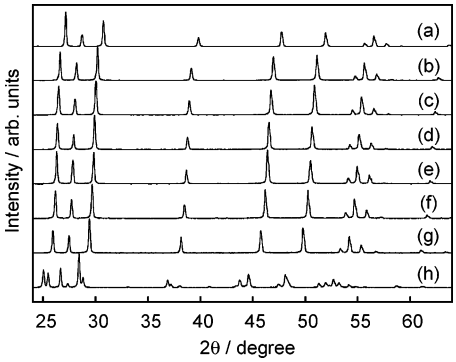


***Figure 2.*** X-ray diffraction patterns of $(AgIn)_xZn_{2(1-x)}S_2$ solid solutions; the values of $x$ are (a) 0, (b) 0.17, (c) 0.22, (d) 0.29, (e) 0.33, (f) 0.40, (g) 0.5, and (h) 1. Preparation condition: (a) heat-treated in a quartz ampule tube at 1323 K and (b)−(h) heat-treated in a $N_2$ flow at 1073−1123 K.

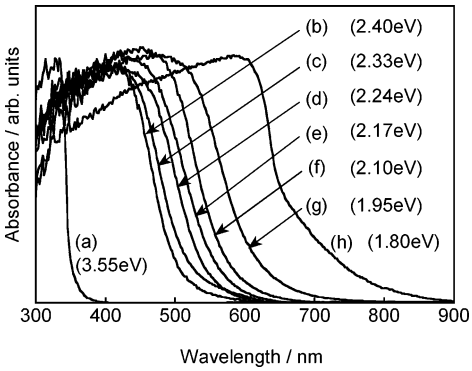


***Figure 3.*** Diffuse reflection spectra of $(AgIn)_xZn_{2(1-x)}S_2$ solid solutions; the values of $x$ are (a) 0, (b) 0.17, (c) 0.22, (d) 0.29, (e) 0.33, (f) 0.40, (g) 0.5, and (h) 1. Preparation condition: (a) heat-treated in quartz ampule tube at 1323 K and (b)−(h) heat-treated in a $N_2$ flow at 1073−1123 K.

CASTEP program to obtain further information on the energy structure of the $(AgIn)_xZn_{2(1-x)}S_2$ solid solutions.[30] The core electrons were replaced with norm-conserving pseudo potential, and the valence electronic configurations for Zn, Ag, In, and S were $3d^{10}4s^2$, $5s^14d^{10}$, $5s^24d^{10}5p^1$, and $3s^23p^4$, respectively. The kinetic energy cutoffs were taken to be 250 and 260 eV for ZnS and $AgInS_2$, respectively. The calculations were carried out using the primitive unit cells of $[ZnS]_2$ and $[AgInS_2]_4$, which had 9 and 36 occupied orbitals, respectively. The atomic coordinates of ZnS and $AgInS_2$ were referenced from Yeh et al.[31] and Krustok et al.,[32] respectively.

## Results and Discussion

**Crystal Structure.** Figure 2 shows X-ray diffraction patterns of the $(AgIn)_xZn_{2(1-x)}S_2$ solid solutions. The single phase of a hexagonal wurtzite structure was obtained for all prepared samples. The diffraction peaks were shifted to a lower-angle side as the value of $x$ increased. The successive shift of the XRD pattern indicated that the crystals obtained were not mixtures of ZnS and $AgInS_2$ phases but $(AgIn)_xZn_{2(1-x)}S_2$ solid solutions. The shift was reasonable because the ion radii of $Ag^+$ (1.14 Å) and $In^{3+}$ (0.76 Å) are larger than that of $Zn^{2+}$ (0.74 Å).[33]

**Photophysical Properties.** Figure 3 shows diffuse reflection spectra of $(AgIn)_xZn_{2(1-x)}S_2$ solid solutions, which had intense absorption bands with steep edges in the visible-light region, being different from ZnS that has a UV absorption band. This shape indicates that the visible-light absorption was due to a band transition, not due to the transition from impurity levels to the conduction band of ZnS as observed for the Ni or Cu-doped ZnS photocatalyst.[5,6] The absorption edge of the $(AgIn)_xZn_{2(1-x)}S_2$ solid solutions was in a position between those of ZnS and $AgInS_2$, and the band gap became narrow monotonically as the value of $x$ increased. The band gaps of the solid solutions were estimated to be 2.40−1.95 eV ($x = 0.17-0.5$) from the onsets of the absorption edges.

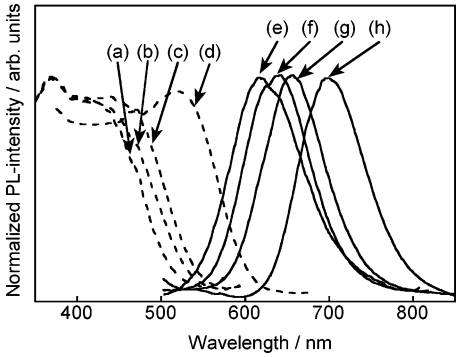


***Figure 4.*** Photoluminescence spectra of $(AgIn)_xZn_{2(1-x)}S_2$ solid solutions at 80 K. Excitation spectra: (a) $x = 0.22$, monitored at 630 nm, (b) $x = 0.29$, monitored at 640 nm, (c) $x = 0.33$, monitored at 655 nm, and (d) $x = 0.5$, monitored at 700 nm. Emission spectra: (e) $x = 0.22$, excited at 415 nm, (f) $x = 0.29$, excited at 420 nm, (g) $x = 0.33$, excited at 445 nm, and (h) $x = 0.50$, excited at 520 nm.

The $(AgIn)_xZn_{2(1-x)}S_2$ solid solutions ($x = 0.22-0.40$) showed photoluminescence at 80 K as shown in Figure 4. The onsets of excitation spectra were in almost the same position as those of diffuse reflection spectra, which indicates that the emission of the $(AgIn)_xZn_{2(1-x)}S_2$ solid solutions was derived from band gap excitation. The photoluminescence spectra of $(AgIn)_xZn_{2(1-x)}S_2$ were shifted successively with a change in the composition as well as in the diffuse reflection spectra. These photophysical properties of absorption and photoluminescence revealed that the energy structure of the $(AgIn)_xZn_{2(1-x)}S_2$ solid solutions depended on the value of $x$.

**Band Structures.** Figure 5a shows the band structures and the densities of states (DOS) of ZnS and $AgInS_2$. Figure 5b shows the density contour maps for the LUMOs (conduction band minimum) and HOMOs (valence band maximum) of ZnS and $AgInS_2$. Most orbitals of ZnS consisted of hybrid orbitals of Zn and S because of the covalency as shown in Figure 5a. The occupied bands of ZnS were classified into three bands. The lower-energy side in the occupied bands consisted of S 3s orbitals (#1 ≈ 2). The side with energy higher than S 3s consisted of Zn 3d (+ S 3p) (#3 ≈ 12) and S 3p (+ Zn 4s4p) bands (#13 ≈ 18). The valence band maximum (HOMO, #18) mainly consisted of slightly hybridized S 3p orbitals and Zn 4s4p orbitals. On the other hand, the conduction band minimum (LUMO, #19) consisted of an antibonding orbital of Zn 4s4p hybridized with a certain quantity of a S 3p orbital. The lower-energy side in the occupied bands of $AgInS_2$ was composed of hybrid orbitals of S 3s + In 4d (#1 ≈ 4) and In 4d orbitals (#5 ≈ 20). The middle part consisted of S 3s orbitals (#21 ≈ 28). The higher-energy side in the occupied bands consisted of In 5s + S 3p (#29 ≈ 32) and S 3p + Ag 4d hybrid orbitals (#33 ≈ 72). The contribution of S 3p increased as the energy became

(30) Payne, M. C.; Teter, M. P.; Allan, D. C.; Arias, T. A.; Joannopoulos, J. D. *Rev. Mod. Phys.* **1992**, *64*, 1045−1097.
(31) Yeh, C. Y.; Lu, Z. W.; Froyen, S.; Zunger, A. *Phys. Rev. B* **1992**, *46*, 10086−10097.
(32) Krustok, J.; Raudoja, J.; Krunks, M. *J. Appl. Phys.* **2000**, *88*, 205−209.
(33) Shannon, R. D. *Acta Crystallogr.* **1976**, *A32*, 751−767.

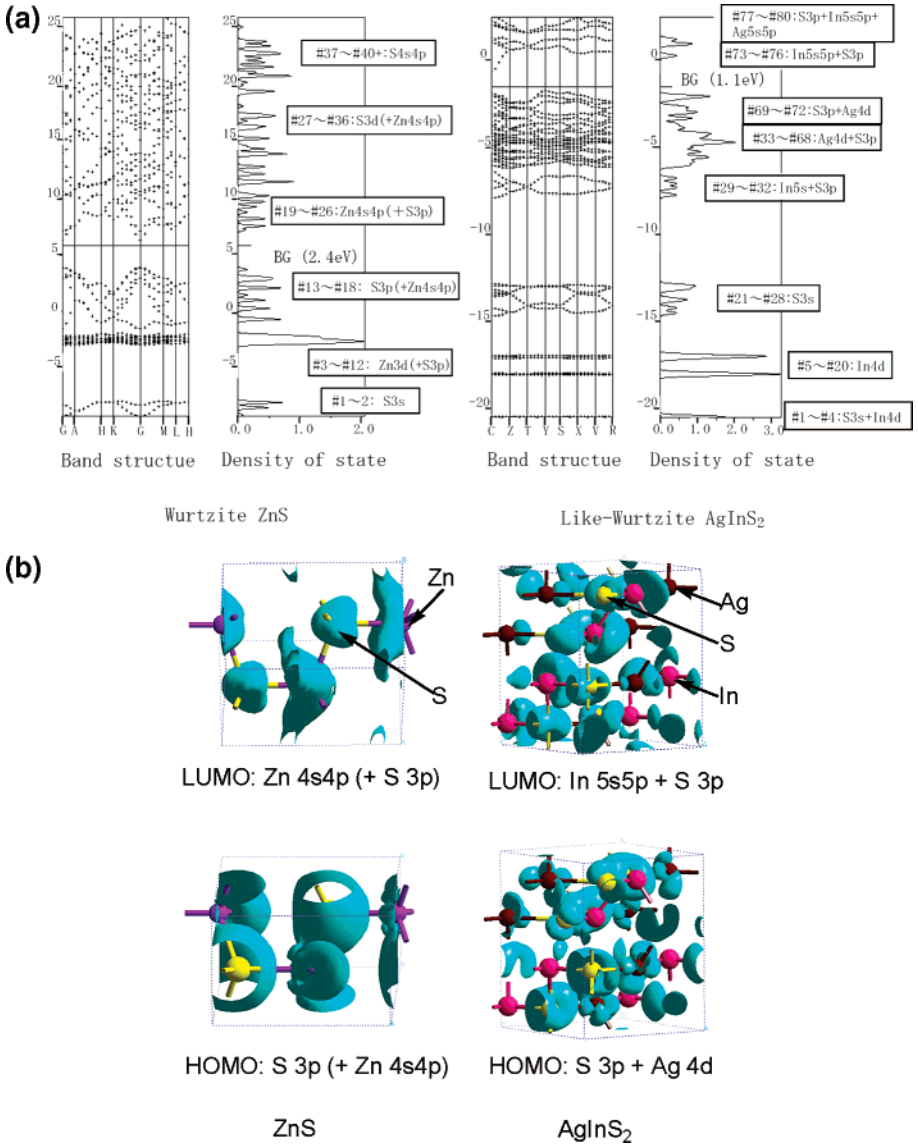


***Figure 5.*** (a) Band structures and densities of states for ZnS and $AgInS_2$ calculated by the density functional method. (b) Density contour maps for the LUMOs and HOMOs of ZnS and $AgInS_2$.

high in the S 3p + Ag 4d hybrid orbitals (#33 ≈ 72). The valence band maximum (HOMO, #72) was made up of hybrid orbitals of S 3p and Ag 4d. The conduction band minimum (LUMO, #73) was composed of In 5s5p hybridized with S 3p orbitals. The lower-energy side in the unoccupied bands was composed of In 5s5p + S 3p hybrid orbitals (#73 ≈ 76). The higher-energy side in the unoccupied bands consisted of S 3p + In 5s5p + Ag 5s5p hybrid orbitals (#77 ≈ 80). The contribution of S 3p orbitals to the conduction band indicates that $AgInS_2$ partly consisted of covalent bands as well as ZnS. The calculated band gap energies of ZnS and $AgInS_2$ were 2.4 and 1.1 eV, respectively.

It was reported from other calculation techniques that the upper part of a valence band of $AgInS_2$ was composed of a d-state of Ag mixed with a p-state of S.[34,35] It is similar to the present result obtained by a plane-wave-based density functional calculation. Moreover, $AgMO_3$ (M = Nb and Ta) photocatalysts have stable valence bands consisting of Ag 4d orbitals.[11] It is remarkable that Ag 4d orbitals are involved in the formation of a valence band even in sulfide.

The photophysical properties and DFT calculations revealed the band structure of the $(AgIn)_xZn_{2(1-x)}S_2$ solid solutions between ZnS and $AgInS_2$, as shown in Figure 6. Both S 3p and Ag 4d orbitals contribute to making up a valence band. The valence band maximum (HOMO) should also be composed of hybrid orbitals of S 3p and Ag 4d, as seen for $AgInS_2$. In 5s5p orbitals mixed with Zn 4s4p contribute to forming a conduction band, and the conduction band minimum (LUMO) should be composed of hybrid orbitals of In 5s5p + Zn 4s4p. A similar hybridization of the In orbital in a conduction band was observed in a $Ga_2O_3-In_2O_3$ solid solution photocatalyst.[17] The positions of HOMO and LUMO of the $(AgIn)_xZn_{2(1-x)}S_2$ solid solutions should be located between those of ZnS and $AgInS_2$. The valence and conduction band levels can be shifted successively by a change in the ratio of $AgInS_2$ to ZnS. The proposed band structure of the solid solution is reasonable judging from continuous shifts in diffuse reflection and photoluminescence

(34) Lavrentiev, A. A.; Gabrelian, B. V.; Nikiforov, I. Y. *J. Struct. Chem.* **2000**, *41*, 418−426.
(35) Rashkeev, S. N.; Lambrecht, W. R. L. *Phys. Rev. B* **2001**, *63*, 165212−165223.

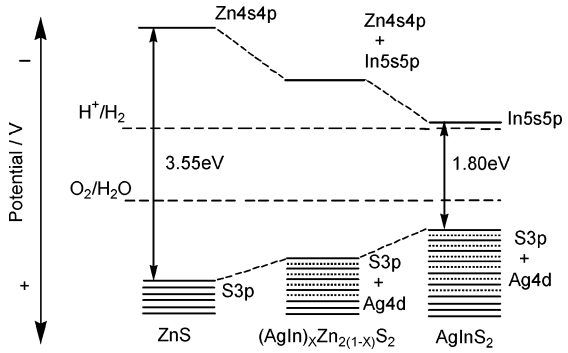


***Figure 6.*** Band structures of $(AgIn)_xZn_{2(1-x)}S_2$ solid solutions, ZnS, and $AgInS_2$.

***Table 1.*** Dependence of Photocatalytic Activities for $H_2$ Evolution from an Aqueous $K_2SO_3$ Solution under Visible Light Irradiation over $(AgIn)_xZn_{2(1-x)}S_2$ Solid Solutions upon the Composition (Value of $x$)[a]

| | | rate of $H_2$ evolution/$\mu$mol $h^{-1}$ | |
|---|---|---|---|
| composition $x$ | band gap (eV) | unloaded | Pt (3 wt %)-loaded |
| 0 | 3.55 | 0.2 | 0.9 |
| 0.17 | 2.40 | 62 | 234 |
| 0.22 | 2.33 | 51 | 424 |
| 0.29 | 2.24 | 96 | 337 |
| 0.33 | 2.17 | 53 | 279 |
| 0.40 | 2.10 | 44 | 238 |
| 0.50 | 1.95 | 5 | 46 |
| 1 | 1.80 | 1.1 | 12 |

[a] Catalysts: 0.3 g, heat-treated in a $N_2$ flow at 1073−1123 K. Reactant solution: 300 mL (0.5 mol $L^{-1}$ $K_2SO_3$). Light source: 300 W Xe lamp with a cutoff filter ($\lambda \geq 420$ nm).

spectra. These observations show that the $(AgIn)_xZn_{2(1-x)}S_2$ solid solutions are promising materials in which the band structure can be controlled. The $(AgIn)_xZn_{2(1-x)}S_2$ solid solution is expected to be a new visible-light-driven photocatalyst if the conduction band level is high enough to reduce $H_2O$ to form $H_2$.

**Dependency of Photocatalytic Activities on Composition.** Table 1 shows the effect of composition on the photocatalytic activities of unloaded and Pt (3 wt %)-loaded $(AgIn)_xZn_{2(1-x)}S_2$ solid solutions for $H_2$ evolution from an aqueous solution containing $SO_3^{2-}$ as a sacrificial reagent under visible-light irradiation. The photocatalytic activities depended upon the composition. $AgInS_2$ and ZnS hardly possessed any activities under visible-light irradiation. In contrast, the solid solutions showed photocatalytic activity for $H_2$ evolution under visible-light irradiation ($\lambda > 420$ nm) even without Pt cocatalysts. This indicates that the conduction band level of the solid solution was higher than the reduction potential of $H_2O$ to form $H_2$ as well as that of the ZnS photocatalyst. The photocatalytic activity increased when the Pt cocatalysts that worked as active sites for $H_2$ evolution were loaded on the $(AgIn)_xZn_{2(1-x)}S_2$ solid solution photocatalysts. When $x$ was 0.22−0.29, the highest activities were obtained for the unloaded and Pt (3 wt %)-loaded photocatalysts. The dependency of the $H_2$ evolution reaction upon the composition would mainly be due to the change in the band structure. The photocatalytic activity increased with the formation of the conduction band that was high enough to reduce $H_2O$ to form $H_2$ as the ratio of ZnS increased. However, the activity for $H_2$ evolution decreased as the value of $x$ became smaller than 0.22. One of the reasons for the low activity might be the decrease in the number of available photons of which the energy was larger than the band gap. However, the difference in the activity cannot be explained only by taking the number of available photons into account because the difference in the number of available photons is not so large. Another possible factor is that In and Ag orbitals form not bands, but discrete levels as the concentrations of their components become low. It would result in the decrease in the mobility of photogenerated carriers, an important factor that affects photocatalytic activity.

***Table 2.*** Effects of Reaction and Preparation Condition on Photocatalytic Activities of $(AgIn)_{0.22}Zn_{1.56}S_2$ Solid Solution[a]

| heat-treatment conditions[b] | reactant solutions | Pt-cocatalyst/ wt % | rate of $H_2$ evolution/$\mu$mol $h^{-1}$ |
|---|---|---|---|
| $N_2$ flow | $K_2SO_3$ aq[c] | none | 51 |
| | $K_2SO_3$ aq[c] | 3 | 424 |
| | $Na_2S$ aq[d] | 3 | 296 |
| | $K_2SO_3 + Na_2S$ aq[e] | none | 72 |
| | $K_2SO_3 + Na_2S$ aq[e] | 3 | 529 |
| sealed quartz ampule tube | $K_2SO_3 + Na_2S$ aq[e] | none | 328 |
| | $K_2SO_3 + Na_2S$ aq[e] | 3 | 944 |

[a] Catalyst: 0.3 g. Reactant solutions: 300 mL. Light source: 300 W Xe lamp ($\lambda \geq 420$ nm). [b] Heat-treated at 1123 K. [c] A solution of 0.5 mol $L^{-1}$ $K_2SO_3$. [d] A solution of 0.1 mol $L^{-1}$ $Na_2S$. [e] A solution of 0.25 mol $L^{-1}$ $K_2SO_3$ + 0.35 mol $L^{-1}$ $Na_2S$.

The solid solution photocatalyst ($x = 0.22$) showed only $H_2$ evolution (35 $\mu$mol $h^{-1}$), no oxygen evolution, for a water splitting reaction without any sacrificial regents. The rate of $H_2$ evolution for water splitting was significantly smaller than that for the sacrificial system. The $H_2$ evolution of water splitting would be due to the photocorrosion.

**Optimization of Reaction and Preparation Conditions.** The $(AgIn)_{0.22}Zn_{1.56}S_2$ solid solution without Pt cocatalysts showed comparatively low activity for $H_2$ evolution, the initial rate of which was 51 $\mu$mol $h^{-1}$. The activity was much improved by loading of the Pt cocatalysts, and the initial rate of $H_2$ evolution became 424 $\mu$mol $h^{-1}$. Unfortunately, the photocatalyst showed observable deactivation after irradiation for 3 h. Therefore, the preparation and reaction conditions were investigated to improve the photocatalytic activities, as shown in Table 2. An aqueous solution containing either $K_2SO_3$ or $Na_2S$ and a mixed solution containing both $K_2SO_3$ and $Na_2S$ as electron donors were employed for reactant solutions. The heat treatment in the preparation of the photocatalyst was carried out in an $N_2$ flow and an evacuated quartz ampule tube. The photocatalytic activity was improved by using the mixed solution containing both $K_2SO_3$ and $Na_2S$ as electron donors. Moreover, observable deactivation during the course of photocatalytic reaction was suppressed. Under this condition, the photocatalytic reaction is supposed to proceed along the following processes:[2,25]

$$\text{Photocatalyst} + h\nu \rightarrow e^-(\text{CB}) + h^+(\text{VB}) \quad (1)$$

$$2H_2O + 2e^-(\text{CB}) \rightarrow H_2 + 2OH^- \quad (2)$$

$$SO_3^{2-} + H_2O + 2h^+(\text{VB}) \rightarrow SO_4^{2-} + 2H^+ \quad (3)$$

$$2S^{2-} + 2h^+(\text{VB}) \rightarrow S_2^{2-} \quad (4)$$

$$S_2^{2-} + SO_3^{2-} \rightarrow S_2O_3^{2-} + S^{2-} \quad (5)$$

$$SO_3^{2-} + S^{2-} + 2h^+(\text{VB}) \rightarrow S_2O_3^{2-} \quad (6)$$

$H_2O$ is reduced to $H_2$ by the electrons photogenerated in the

conduction band accompanied by oxidation of sacrificial reagents. The photogenerated holes in the valence band oxidize $SO_3^{2-}$ and $S^{2-}$ to form $SO_4^{2-}$ and $S_2^{2-}$ directly, according to eqs 3 and 4, respectively. The production of $S_2^{2-}$ ions, which act as an optical filter and compete with the reduction of protons, was efficiently suppressed by mixing with $SO_3^{2-}$ ions, according to eqs 5 and 6. The presence of excess $S^{2-}$ ions in the reaction solution also stabilizes the photocatalyst surface because the formation of sulfur defects could be suppressed. The activity from the aqueous solution containing only $Na_2S$ over the Pt-loaded $(AgIn)_{0.22}Zn_{1.56}S_2$ photocatalyst was lower than that under any other reaction conditions and was significantly deactivated. This is due to the formation of $S_2^{2-}$ ions in the reactant solution.

Sulfur, zinc, and indium could be easily volatilized during the synthesis process of heat treatment in the $N_2$ flow. Therefore, in the preparation, Ag−In−Zn sulfide precursors were heat-treated in an evacuated quartz ampule tube to prevent volatilization. It should be noted that the $(AgIn)_{0.22}Zn_{1.56}S_2$ photocatalyst heat-treated in this condition showed high activity even without Pt cocatalysts (328 $\mu$mol $h^{-1}$), different from the well-known CdS photocatalyst. The photocatalytic activity was about five times higher than that heat-treated in the $N_2$ flow. Ag (1 wt %) metals were loaded on the photocatalyst by a photodeposition method to see if the Ag metal could be an efficient cocatalyst for $H_2$ evolution. The activity of the Ag-loaded photocatalyst was lower than that of an unloaded photocatalyst. This result means that, even if some surface silver cations are photoreduced to metallic silver, they cannot act as cocatalysts for $H_2$ evolution sites. The ability to generate $H_2$ without Pt cocatalysts is due to the high conduction band level. The catalyst with a photodeposited Pt cocatalyst showed the highest activity (944 $\mu$mol $h^{-1}$), and the steady activity was obtained after ca. 5 h. The activity of a Pt-loaded photocatalyst was doubled by the heat treatment. The turnover number, which was obtained as the ratio of the amount of reacted electrons to that of a molar quantity of the used $(AgIn)_{0.22}Zn_{1.56}S_2$ photocatalyst (0.3 g), was 54 at 14 h, at which the activity was still steady.[29] The turnover number indicates that the reaction proceeded photocatalytically. As a reference, the rate of $H_2$ evolution on a Pt-loaded CdS photocatalyst was 358 $\mu$mol $h^{-1}$ under the same experimental condition. The reason the heat treatment in an ampule tube improved the photocatalytic activity was due to the suppression of defect formation because the defect formed by volatilization of elements acts as a recombination center between the photogenerated electrons and holes. However, a slight deactivation was still observed at the initial stage even under the optimized condition. The poisoning of a Pt cocatalyst with sulfur and the change of the surface in an atomic level are possible causes for the deactivation although the remarkable changes in XRD patterns and electron micrograph images were not confirmed before and after the reaction.

**$H_2$ Evolution under Optimized Conditions.** Figure 7 shows an action spectrum for $H_2$ evolution from an aqueous solution containing both $K_2SO_3$ and $Na_2S$ over the Pt (3 wt %)-loaded $(AgIn)_{0.22}Zn_{1.56}S_2$ solid solution photocatalysts heat-treated in an ampule tube. The onset of the action spectrum agreed well with that of the diffuse reflection spectrum. $H_2$ evolution did not appear by absorption in the tail region (550−650 nm). It was revealed that the visible-light response of the photocatalyst was due to the band gap transition between the valence and

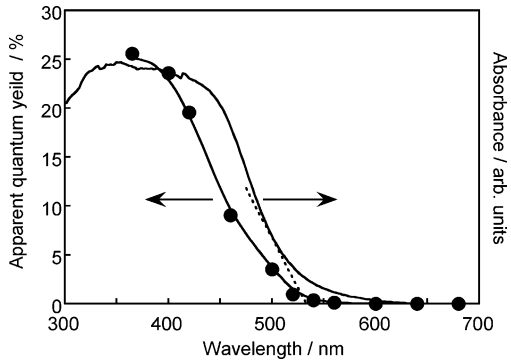


***Figure 7.*** Action spectrum of $H_2$ evolution from an aqueous $K_2SO_3$ (0.25 mol $L^{-1}$)−$Na_2S$ (0.35 mol $L^{-1}$) solution (300 mL) over the Pt (3 wt %)-loaded $(AgIn)_{0.22}Zn_{1.56}S_2$ solid solution heat-treated in a quartz ampule tube at 1123 K. Catalyst: 0.3 g. Light source: 300 W Xe lamp with cutoff and band pass filters. Reaction cell: side window Pyrex cell.

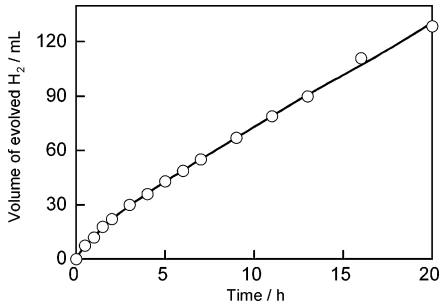


***Figure 8.*** Photocatalytic $H_2$ evolution from an aqueous $K_2SO_3$ (0.25 mol $L^{-1}$)−$Na_2S$ (0.35 mol $L^{-1}$) solution (150 mL) under a simulated sunlight irradiation over the Pt (3 wt %)-loaded $(AgIn)_{0.22}Zn_{1.56}S_2$ solid solution heat-treated in a quartz ampule tube at 1123 K. Catalyst: 0.3 g. Solar simulator: 300 W Xe short arc lamp with AM-1.5 filter. Reaction cell: top window Pyrex cell. Irradiated area: 33 $cm^2$.

conduction bands that were controllable by making a solid solution. The quantum yield of the Pt-loaded $(AgIn)_{0.22}Zn_{1.56}S_2$ photocatalyst was 20% at 420 nm, which was quite high even considering the presence of the sacrificial agents. Only the Pt-loaded CdS photocatalyst shows a higher quantum yield (QY = 37%), but it includes harmful cadmium and always requires the Pt cocatalyst.

Figure 8 shows $H_2$ evolution under simulated sunlight irradiation (AM 1.5) from an aqueous solution containing sacrificial reagents, $SO_3^{2-}$ and $S^{2-}$, over a Pt (3 wt %)-loaded $(AgIn)_{0.22}Zn_{1.56}S_2$ solid solution photocatalyst heat-treated in an ampule tube. In this case, the amount of $H_2$ gas evolved was determined by volumetric measurement. Even under simulated sunlight irradiation, the solid solution showed high activity for $H_2$ evolution, the initial rate of which was 11 mL $h^{-1}$ (3.3 L $m^{-2}\cdot h^{-1}$). Steady activity for $H_2$ evolution (1.8 L $m^{-2}\cdot h^{-1}$) was observed after a few hours.

**Role of Surface Morphology.** Figure 9 shows the SEM images of unloaded and Pt-loaded $(AgIn)_{0.22}Zn_{1.56}S_2$ solid solutions. Well-crystallized particles with ca. 10 $\mu$m of size were observed as shown in Figure 9a. The surface area of the solid solution was 0.5 $m^2$ $g^{-1}$. Specific nanostep structures were observed on some parts of a particle's surface, as shown in Figure 9b. Figure 9, parts c−e, shows the surface structures of Pt 1 wt %- and 3 wt %-loaded $(AgIn)_{0.22}Zn_{1.56}S_2$ powders. The Pt particles were rapidly photodeposited at the initial stage of the photocatalytic reaction. The Pt nanoparticles were selectively

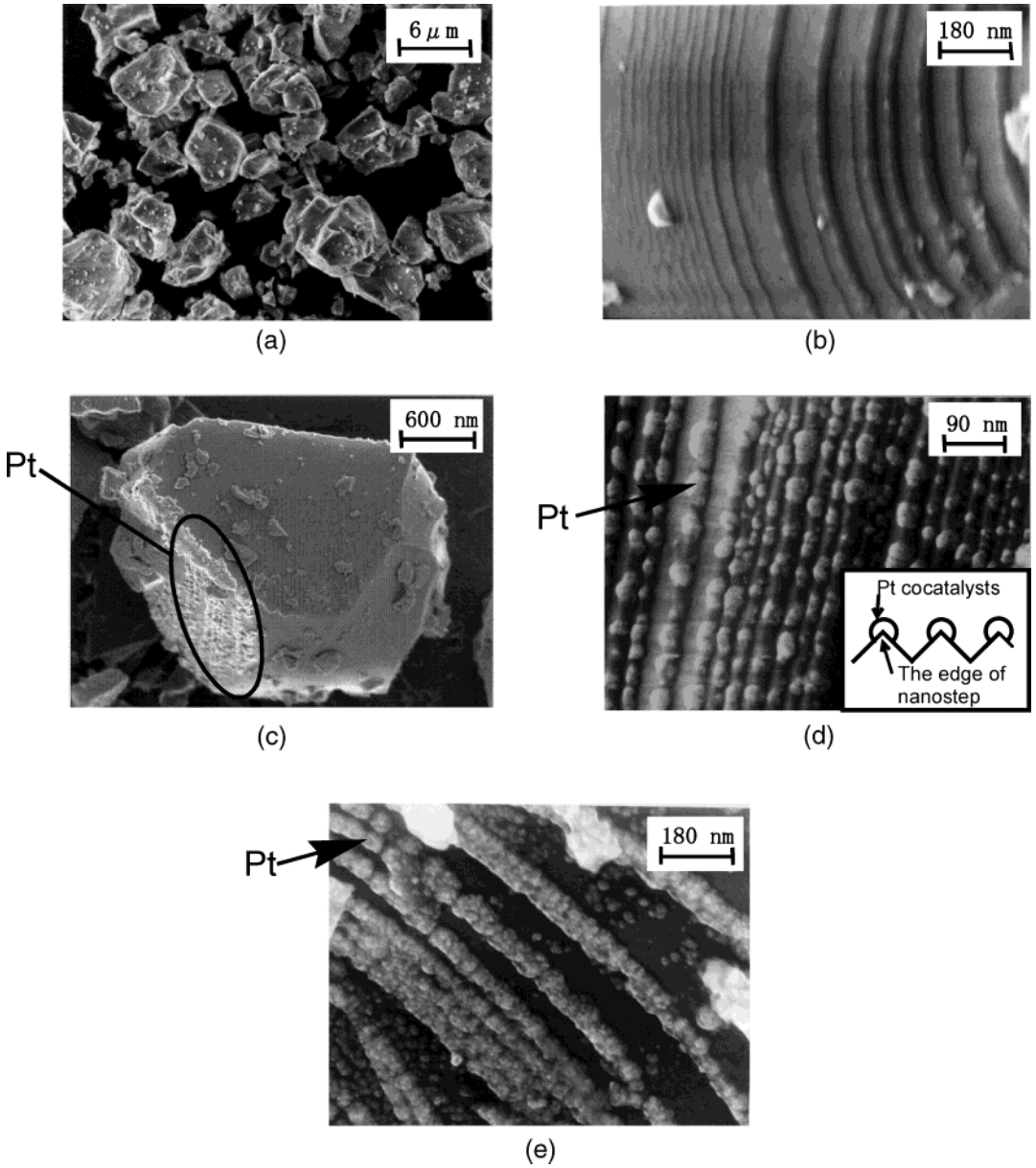


***Figure 9.*** Scanning electron microscope images of the $(AgIn)_{0.22}Zn_{1.56}S_2$ solid solution heat-treated in a $N_2$ flow at 1123 K. (a) and (b) Unloaded, (c) and (e) Pt 3 wt % cocatalyst was loaded, and (d) Pt 1 wt % cocatalyst was loaded.

loaded on the edges of nanosteps on some part of a particle's surface, as shown in Figure 9c. Furthermore, the Pt nanoparticles were deposited at regular intervals along the edges of nanostep in the 1 wt % Pt-loaded sample, as shown in Figure 9d. Moreover, the Pt nanoparticles contacted each other to form nanobeads over the edges of nanostep in the Pt 3 wt %-loaded sample, as shown in Figure 9e. The $H_2$ evolution of Pt 3 wt %-loaded photocatalyst showed higher activity (424 $\mu$mol $h^{-1}$) than that of Pt 1 wt %-loaded photocatalyst (335 $\mu$mol $h^{-1}$) in an aqueous $K_2SO_3$ solution (0.5 mol $L^{-1}$). This result means that Pt cocatalysts of 3 wt % loading still work as the efficient active site rather than the shielding for incident photons. Figure 10a shows a TEM image of a Pt-loaded nanostep structure. The Pt nanoparticles were arranged orderly at ca. 100- to 120-nm intervals. The selective deposition of Pt implied that photogenerated electrons could readily migrate to the edge of the surface nanostep. TEM-EDS analyses revealed that the signals assigned to Pt were clearly observed only at the black spots (A) on the nanosteps, as shown in Figure 10b. In contrast, the signals of Pt were not observed at the unloaded positions (B). Moreover, it was found that the signals assigned to Ag and In were observed more remarkably at point (A) than at point (B). This indicates that Pt nanoparticles tend to be deposited selectively at a certain position, rich in Ag and In.

These nanosteps were self-constructed during a heat treatment of Ag−In−Zn sulfide precursors. The mechanism of the growth is not clear at the present stage. The solid solution would be composed of (Ag,In)-rich and Zn-rich planes in a wurtzite structure, and the cleaved surfaces should form nanosteps, which is suggested by TEM analysis.

We have reported that NiO of the $NiO/NaTaO_3$ photocatalyst doped with lanthanum that showed high photocatalytic activity

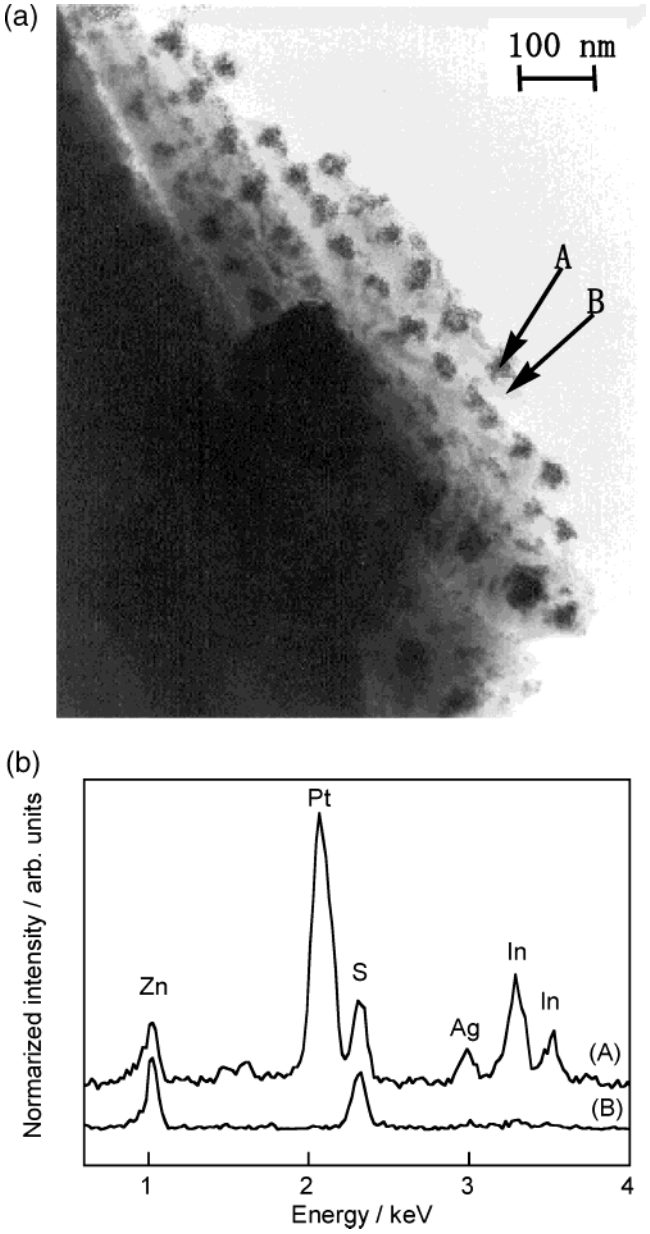


***Figure 10.*** (a) Transmission electron microscope image of Pt 3 wt %-loaded $(AgIn)_{0.22}Zn_{1.56}S_2$ solid solution heat-treated in an $N_2$ flow at 1123 K. (b) Energy-dispersive X-ray spectra of the $(AgIn)_{0.22}Zn_{1.56}S_2$ solid solution.

for water splitting was deposited as ultrafine particles on an ordered surface nanostep structure.[36] The reduction and oxidation sites were effectively separated by the step structure, and the recombination of photogenerated electrons and holes was suppressed. Therefore, it is possible that the specific surface nanostructure of the $(AgIn)_xZn_{2(1-x)}S_2$ solid solution photocatalyst also contributes to the separation of reaction sites and the enhancement of charge separation. In addition, the selective loading of Pt cocatalysts induced a further effective charge separation. Most of Pt particles were selectively deposited on the nanosteps even though a small amount of Pt particles was randomly deposited on the flat surface. This indicates that the reaction for $H_2$ evolution should proceed even over the surfaces without nanosteps. However, the efficiency of $H_2$ evolution on the nanostep surface would be higher than that on the flat surface because Pt cocatalysts were deposited on the nanostep surface much more than the flat surface.

## Conclusions

It was found that $(AgIn)_xZn_{2(1-x)}S_2$ is an active photocatalyst for $H_2$ evolution under visible-light irradiation even though it is the solid solution between $AgInS_2$ and ZnS that hardly possesses any activity under visible-light irradiation. The energy structure (band position) of the solid solution was controllable by a change in composition. DFT calculations indicated that Ag and In took part in the valence band formation and the conduction band formation, respectively. The photocatalytic activity depended on the composition, and Pt (3 wt %)-loaded $(AgIn)_{0.22}Zn_{1.56}S_2$ showed the highest activity. The quantum yield of the photocatalyst was 20% at 420 nm. The present results indicate that control of the energy structure by making a solid solution is a useful strategy for band engineering to develop a visible-light-driven photocatalyst. Moreover, the photocatalysts possessed a specific surface nanostep structure, which works for the separation of active sites and induces the selective loading of Pt nanoparticles. These sulfide photocatalysts that show high activity for $H_2$ evolution are expected to turn into practical application for $H_2$ gas production using byproducts such as hydrogen sulfide emitted by a hydrogenated desulfurization process at petrochemical plants.

**Acknowledgment.** This work was supported by Core Research for Evolutional Science and Technology (CREST), a Grant-in-Aid for the Priority Area Research (No. 417) from the Ministry of Education, Culture, Science, and Technology, and the Tokyo Ohka Foundation for the Promotion of Science and Technology.

JA048296M

(36) Kato, H.; Asakura, K.; Kudo, A. *J. Am. Chem. Soc*. **2003**, *125*, 3082−3089.